Journal of Fluids and Structures 84 (2019) 199–217

Contents lists available at ScienceDirect

Journal of Fluids and Structures

journal homepage: www.elsevier.com/locate/jfs

An experimental investigation into non-linear wave loading on horizontal axis tidal turbines

S. Draycott [a,*], G. Payne [b], J. Steynor [a], A. Nambiar [a], B. Sellar [a], V. Venugopal [a]

[a] School of Engineering, Institute for Energy Systems, The University of Edinburgh, Edinburgh, EH9 3DW, UK
[b] Naval Architecture, Ocean and Marine Engineering, University of Strathclyde, Glasgow, G4 0LZ, UK

ARTICLE INFO

Article history:
Received 20 July 2018
Received in revised form 10 October 2018
Accepted 2 November 2018
Available online xxxx

Keywords:
Tidal stream turbine
Wave loading
Wave–current interaction
Non-linear waves
Scale model testing

ABSTRACT

Tidal turbines are subject to large hydrodynamic loads from combinations of currents and waves, which contribute significantly to fatigue, extreme loading and power flow requirements. Physical model testing enables these loads and power fluctuations to be assessed and understood in a controlled and repeatable environment. In this work, a 1:15 scale tidal turbine model is utilised to further the fundamental understanding of the influence of waves on tidal turbines. A wide range of regular waves are generated in both following-current and opposing-current conditions. Wave frequencies range from 0.31 Hz to 0.55 Hz & wave heights from 0.025 m to 0.37 m in a fixed 0.81 m/s current velocity. Waves are selected and programmed specifically to facilitate frequency domain analysis, and techniques are employed to isolate the effect of non-linear waves on turbine power and thrust.

Results demonstrate that wave action induces large variations in turbine power and thrust compared to current only conditions. For the range of conditions tested, peak values of thrust and power exceed current-only values by between 7%–65% and 13%–160% respectively. These wave-induced fluctuations are shown to increase with wave amplitude and decrease with wave frequency. Following wave conditions exhibit greater variations than opposing for waves with the same wave height and frequency due to the lower associated wavenumbers.

A model is developed and presented to aid the understanding of the high-order harmonic response of the turbine to waves, which is further demonstrated using steady state coefficients under assumptions of pseudo-stationarity. This approach is proven to be effective at estimating wave-induced power and thrust fluctuations for the combinations of waves, currents and turbine state tested. The outcome of which shows promise as a rapid design tool that can evaluate the effect of site-specific wave–current conditions on turbine performance.

1. Introduction

Tidal stream power is a highly dense renewable energy source, which is both predictable and reliable. Recent studies suggest that the theoretical available tidal power, in the UK alone, is 95 TWh/year (The Crown Estate, 2012), yet at present the tidal resource remains largely unexploited. To take advantage of the resource potential, Tidal Stream Turbine (TST) devices have been actively developed, with the first arrays currently being installed and commissioned (Atlantis, 2017).

* Corresponding author.
E-mail address: S.Draycott@ed.ac.uk (S. Draycott).

https://doi.org/10.1016/j.jfluidstructs.2018.11.004

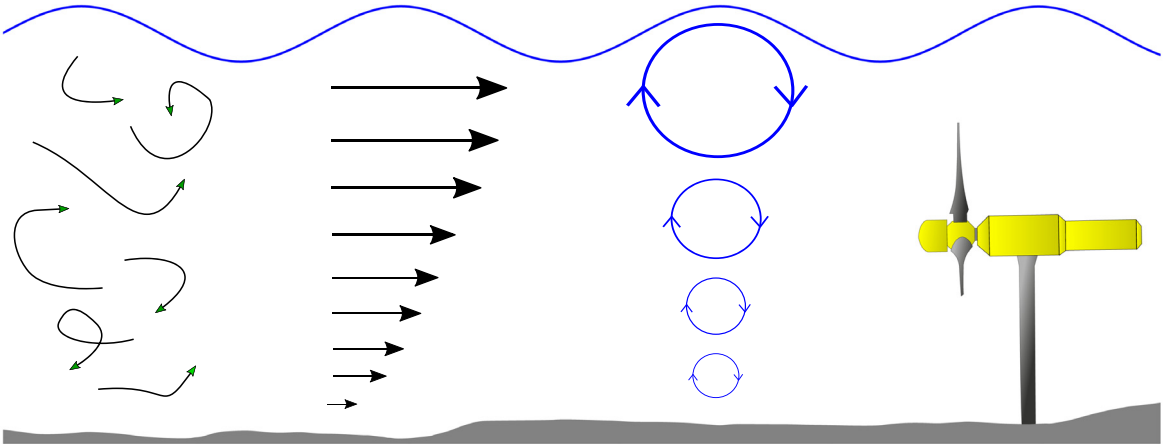

Fig. 1. Diagram of the causes of unsteady loads on tidal turbines. Shown from left to right: turbulence, shear flow and waves.

For farms of devices to be viable, TSTs will need to survive large hydrodynamic loads during their lifetime. Sites with high flow velocities are typically targeted by developers, with notably fast flows occurring in the Pentland Firth, UK, and at Raz Blanchard, France, which feature peak flows in excess of 5 m/s (Draper et al., 2014). In addition to large steady loads resulting from these high mean current flows, unsteady loads from turbulence, waves and shear flow (Milne et al., 2010; MacEnri et al., 2013; Milne et al., 2017) will cause fatigue in TST components, and determine the maximum expected loads for structural design. These unsteady loads are depicted in Fig. 1. The unsteady wave-induced velocities can be several orders of magnitude larger than those resulting from turbulence (Lust et al., 2013).

The importance of unsteady wave loading at tidal stream power sites is well communicated in industrial standards and guidance documents. The International Electrotechnical Commission (IEC) recommends that waves are considered in resource characterisation process (IEC TS 62600-201:2015, 2015), and additionally advises wave measurement programmes where wave orbital velocities are likely to be greater than 20% of the rated current speed (IEC TS 62600-200:2013, 2013). However, there is no defined standard for the prediction of unsteady wave loading on TSTs.

Several previous experimental and simulation studies have investigated TST performance and structural loading in the presence of surface gravity waves, with the vast majority focusing on regular waves. The power and thrust performance of scaled turbines under regular waves superimposed on the current were analysed in De Jesus Henriques et al. (2014), Gaurier et al. (2013), Lust et al. (2013) and Luznik et al. (2013). As expected, mean values were found to be comparable to current-only conditions, yet standard deviations were much greater; up to 40% of their mean values (Gaurier et al., 2013). These significant variations have large implications for the design and operation of TST devices. The variation of turbine loading with respect to wave phase and turbine depth were discussed in Lust et al. (2013) and Luznik et al. (2013). Experimental studies with a scaled device to examine the effects of turbine yaw and wave frequency and amplitude on turbine performance were reported in Galloway et al. (2014). The data obtained from this work and through the work discussed in Barltrop et al. (2006), Faudot et al. (2012) and Guo et al. (2018) were also used to validate advanced Blade Element Momentum Theory (BEMT) codes, which considered the effects of wave loading. A set of experiments to study the out-of-plane root bending moments in attached flows, using an idealised representation of the unsteadiness imparted by turbulence and wave action were reported in Milne et al. (2013) and Milne et al. (2015). These publications informed blade designers with a relatively simple technique to study fatigue loadings due to oscillations of different frequencies on tidal turbines. The work described in Fernandez-Rodriguez et al. (2014) explored extreme thrusts experienced by a scaled TST and reported peak thrust forces close to 2.25 times the mean thrust force for large waves opposing the current. A Computational Fluid Dynamics (CFD) study of the effects of waves on turbine loading and performance, along with blade fatigue life, was presented in Tatum et al. (2016).

This work extends the understanding of wave-induced loads on tidal turbines through experimental investigation using a 1:15 scale, speed-controlled, TST. A wide variety of wave conditions are assessed in a single input current velocity, isolating the fundamental influence of wave frequency and amplitude for waves both following and opposing the current. The effect of opposing waves on turbine loads is not particularly well documented. However, due to flow bidirectionality in tidal channels, waves are likely to oppose the current direction around half the time, and hence are a focus of the presented tests. The analysis of the subsequent results is aided significantly by a frequency-domain methodology presented, whereby the fundamental and higher harmonics corresponding to wave-induced loads are extracted from measured turbine load and power spectra. The understanding gained through the presented analysis of turbine loads in regular wave conditions will subsequently facilitate future work in understanding more complex loading in irregular waves.

The article is laid out as follows: The methodology is described in Section 2, where the TST model turbine, test facility and instrumentation are first described in Sections 2.1 and 2.3. The sea state definition approach is detailed in Section 2.5,

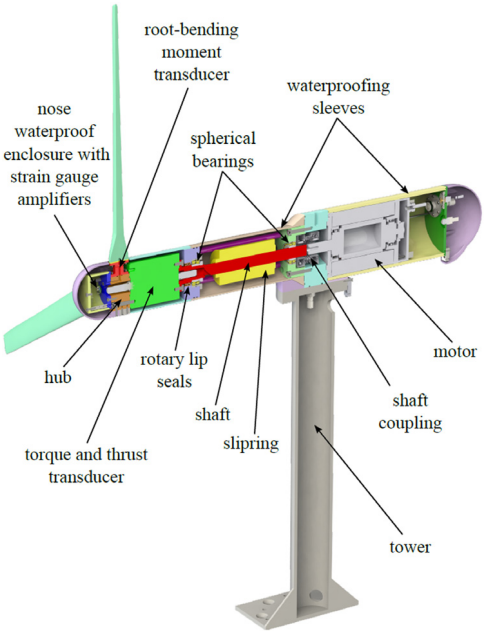

Fig. 2. CAD section view of the experimental turbine model (Payne et al., 2017).

which enables the frequency-domain calculations described in Section 3.2 to be effective. A theoretical analysis of expected harmonic power and thrust response is detailed in Section 3.2, with a step-by-step description of how this analysis can provide power and thrust estimates presented in Section 3.3. Results of wave-induced power and thrust variations identified in the frequency domain are presented in Sections 4.2 and 4.3. Further discussion is offered in Section 5, with concluding remarks made in Section 6.

2. Experimental configuration and test methodology

This section describes the test configuration and methodology including a description of the TST model (Section 2.1), the FloWave wave–current basin (Section 2.2), and the instrumentation layout (Section 2.3). The sea state definition methodology is detailed in Section 2.5 with the resulting test plan described in Section 2.6.

2.1. The model turbine

The TST model is 1:15 scale, has a three-bladed horizontal axis rotor and is bottom-mounted. The rotor diameter, D, is 1200 mm with the turbine rotor axis 1 m from the bed. The bottom-mounted configuration in the test-tank both minimises disruption to the generated wave field and corresponds to the majority of full scale prototypes being currently developed/deployed (see Parkinson and Collier, 2016; MayGen Ltd., 2016 for example). The model is fitted with load sensors measuring flapwise root bending moment (RBM) for each blade and torque (Q) and thrust (T) on the overall rotor. The flapwise root bending moment, equivalent to the streamwise root bending moment when the turbine is aligned to the flow, is the moment measured about an axis parallel to the rotor plane. These load sensors are located 'upstream', in terms of load path, of the shaft seal so that their measurements are not affected by the seal parasitic friction. The generator is simulated by a brushless permanent magnet motor fitted with an encoder measuring the absolute angular position of the rotor. The motor is directly connected to the rotor shaft in 'direct drive' fashion. The blades are designed to produce a rotor thrust coefficient C_T versus tip speed ratio (λ) curve similar to a full scale generic turbine. A detailed description of the turbine and of its instrumentation can be found in Payne et al. (2017) but for convenience, a CAD section view of the model is reproduced in Fig. 2.

The turbine motor was operated in speed control mode with the rotational velocity, ω set to 90 rpm = 9.42 rad/s: corresponding to a nominal tip-speed ratio, λ, of 7. The motor controller was tuned for the wave conditions tested and was found to maintain speed with a variance between 1.18–1.59% depending on the wave conditions.

2.2. The test facility

All the experimental work discussed in this paper, was carried out at the FloWave Ocean Energy Research Facility, located at the University of Edinburgh (UoE), UK (Ingram et al., 2014). Relevant publications studying wave–current interaction at

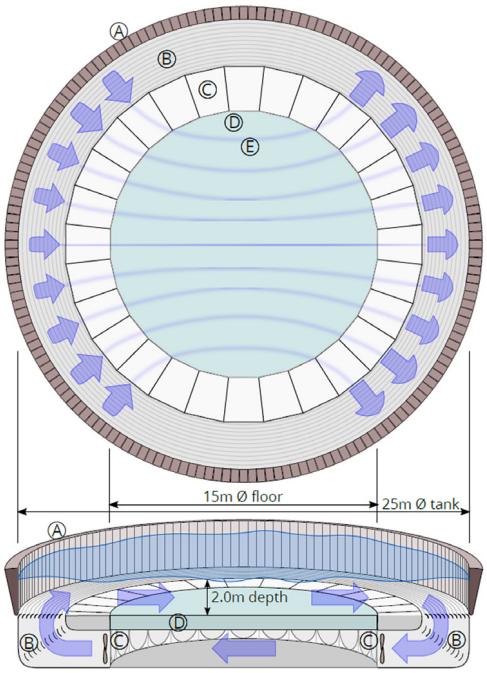

Fig. 3. Schematic of FloWave in plan and oblique section (from Sutherland et al., 2017) showing: (A) Wavemaker paddles around circumference (168 Nr); (B) Turning vanes and flow conditioning filters; (C) Current drive impeller units (28 Nr); (D) Buoyant raisable floor (15 m∅) below test area; (E) Idealised streamlines of flow across tank floor.

Table 1
Description of installed instrumentation including position relative to the turbine rotor plane centre.

Type	Model	Variables measured	Sample rate	Rel. location [m]		
			[Hz]	X	Y	Z
Acoustic Doppler Velocimeter (ADV)	Vectrino profiler	U, V, W	100	−2.40	0	0.60
Wave gauge	FloWave	η	128	0	0	–
TST instrumentation	University of Edinburgh	T, Q, RBM, θ	256	0	0	0
Load cell	AMTI OR6–7	$F_X, F_Y, F_Z,$ M_X, M_Y, M_Z	256	0.49	0	−1.00

FloWave can be found in Draycott et al. (2017, 2018), whilst details of turbulence and flow characterisation are available in Sutherland et al. (2017).

The facility, depicted in Fig. 3, is a circular, combined wave and current basin, with a diameter of 25 m and a nominal water depth of 2 m. There are 168 active-absorbing force-feedback wavemakers around the entire circumference of the facility that are used to generate waves. Mounted in the plenum chamber beneath the floor are 28 impeller units that are used to create a re-circulating flow system. The arrangement of impellers and wavemakers at the facility allows the generation of a predominantly straight flow in any direction across the central test area and enables waves to be added to the current field at any relative angle. The frequency range of the waves that can be generated is between 0.2–1.2 Hz with a maximum wave height of 0.45 m attainable at 0.5 Hz. The maximum current velocity achievable is 1.6 m/s.

The 1.2 m diameter turbine, when installed in this facility, has a blockage ratio of 2.26%. Given the circular nature of the basin this is calculated as the swept area of the turbine divided by the cross sectional area at the centre of the tank.

2.3. Instrumentation and configuration

In addition to the sensors integrated into the TST model (Section 2.1), additional instrumentation was installed throughout the test volume as summarised in Table 1. This includes a resistance-type wave gauge to measure water surface elevation, an Acoustic Doppler Velocimeter (ADV) to measure current velocity, and a bottom-mounted six-axes (6-DOF) load cell to measure forces, F, and moments, M, on the entire TST structure (blades, TST body and tower). The test set-up is illustrated in Fig. 4, where the turbine is depicted to scale in conjunction with the installed instrumentation.

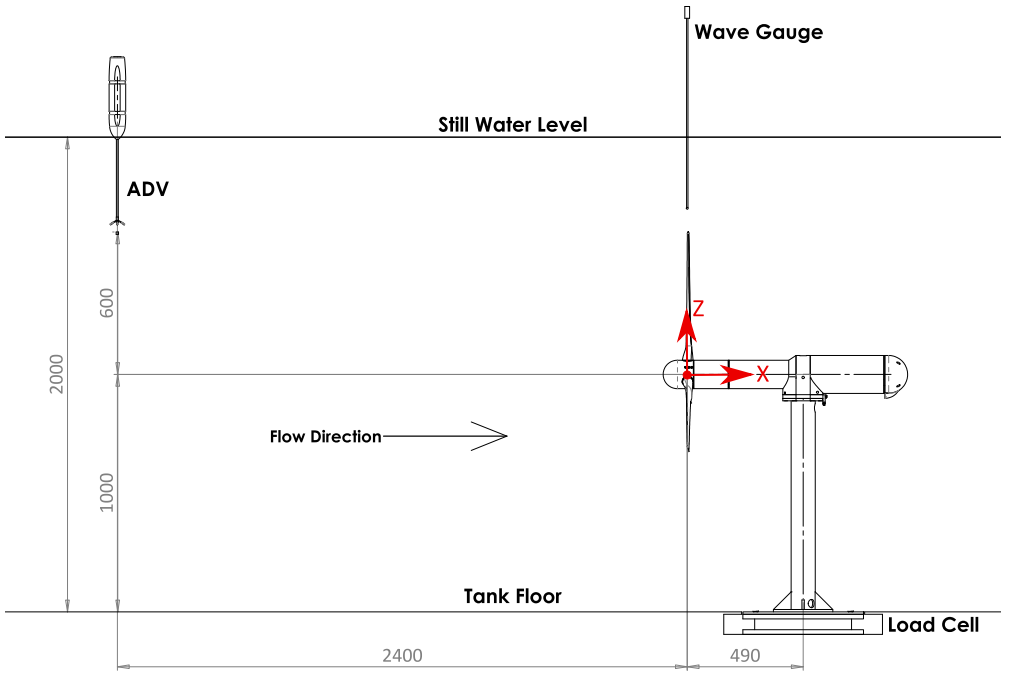

Fig. 4. Location of test instrumentation in the FloWave basin relative to the rotor plane (dimensions in mm).

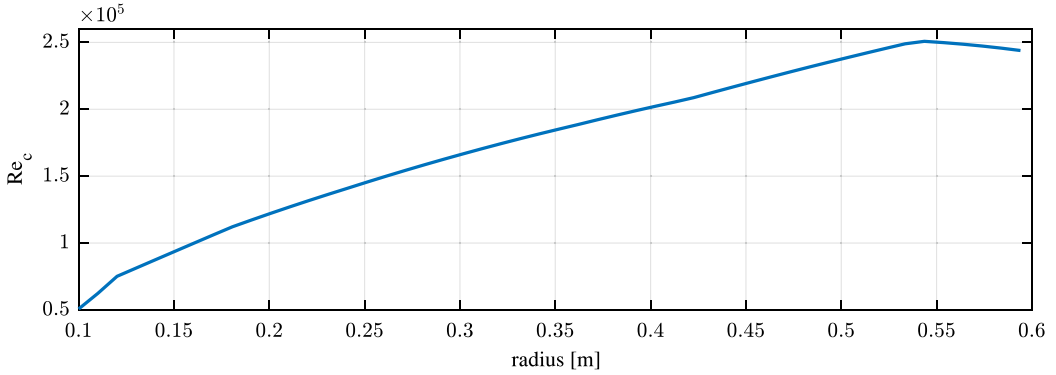

Fig. 5. Chord based Reynolds number variation with local radius.

2.4. Reynolds and froude numbers

The Reynolds and Froude numbers specified in this section are based on the mean onset flow velocity $\bar{U}$ = 0.81 m/s, and do not account for the wave induced velocity.

The rotor diameter based Reynolds number is given by:

$$Re_D = \frac{\rho \cdot \overline{U} \cdot D}{\mu} \tag{1}$$

where ρ and μ are the water density and kinematic viscosity respectively. $Re_D = 975\,000$ throughout the study presented herein.

The blade chord based Reynolds number is calculated based on rotor rotational velocity:

$$Re_c(r) = \frac{\rho \cdot \omega \cdot r \cdot c(r)}{\mu} \tag{2}$$

where r is the local radius and $c(r)$ the corresponding local blade chord length. Fig. 5 shows the variation of Re_c with radius.

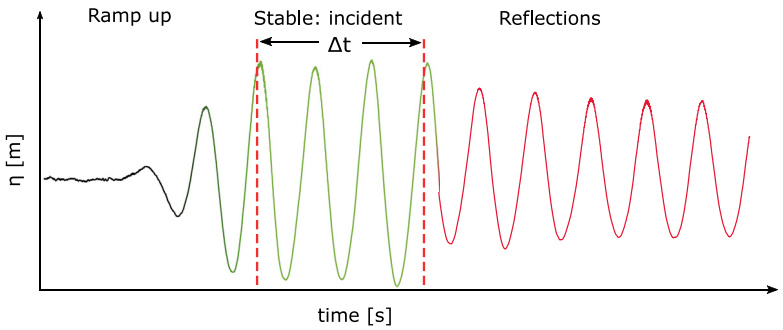

Fig. 6. Example of a stable region of waves used for snippet analysis. Ramp up, stable and regions with reflections shown.

The Froude number of the test facility is given by:

$$Fr = \frac{\overline{U}}{\sqrt{gh}} \tag{3}$$

where g is the gravitational acceleration and h the channel water depth. For the experiments reported in this article, $Fr = 0.18$.

2.5. Defining and producing sea states

2.5.1. Effective sea state definition

The aim of these tests is to use monochromatic 'regular' waves to gain an insight into the fundamental TST response in simple wave–current conditions. It is therefore important to isolate the turbine response to the desired wave conditions from other sources such as turbulence and reflected waves. The approach adopted to achieve this is to rely on Fourier analysis of load time series to isolate to frequency components associated with the regular wave frequency. Moreover, it is necessary to identify a 'snippet' within each test, Δt, which corresponds to a stable region of the time series. This is illustrated in an exaggerated manner in Fig. 6. This approach ensures that the desired wave heights have been attained (out of ramp-up period), and that there are no interfering wave-induced velocity components from reflected waves. Note that in Fig. 6 wave heights are reduced once reflections are present, which is an example of a destructive interference location. The partial standing wave formed will cause varying degrees of constructive and destructive interference spatially.

Choosing a time-period, such as depicted in Fig. 6, which removes the effect of reflection enables more accurate results to be inferred from the tests. Further considerations can also improve the quality of the Fourier analysis. If the generation wave frequency, f_i, is chosen with the likely Δt in mind (from theoretical group velocities in current), and vice versa, then it can be guaranteed that the snippet duration is equal to an exact integer number of wave cycles. This is highly desirable for the Fourier analysis of the corresponding time series as it minimises spectral leakage on the frequency components associated with wave induced loads (see Payne et al., 2009 for more detail).

For deterministic wave generation systems, such as those developed by Edinburgh Designs Ltd. and utilised in FloWave, the frequency increments used to define sea state are defined by the repeat time, T_R, of the sea state. The repeat time defines the test length required to obtain the desired spectrum, ensuring every wave frequency present has undergone an integer number of cycles. The lowest frequency available, and hence the resulting frequency resolution, Δf, is then simply the reciprocal of the repeat time as shown in Eq. (4):

$$\Delta f = \frac{1}{T_R} \tag{4}$$

When generating a regular wave the frequency chosen, f_i, must be an integer multiple, M, of these frequency increments:

$$f_i = M\Delta f \tag{5}$$

To ensure the chosen frequency will correspond exactly to a frequency component of the Fourier analysis, the snippet must include an integer number, N, of the wave period, T_i:

$$\Delta t = NT_i = \frac{N}{f_i} = \frac{N}{M\Delta f} \tag{6}$$

If Eq. (6) is not satisfied for all frequency components of interest, as will be the case in real ocean conditions, then spectral leakage will occur and component amplitudes resulting from an FFT are no longer as useful for comparison. All the combinations of wave periods and snippet durations used for the experiments presented in this article were chosen so that they satisfy equation (6). The final wave specifications and test plan are described in Section 2.6.

Table 2
Regular wave frequencies chosen to keep repeat times small, along with resulting snippet times used ensuring no reflections are present.

Target frequency [Hz]	Obtained frequency f_i [Hz]	Repeat time T_R [s]	Following wave snippet times Δt [s]	Opposing wave snippet times Δt [s]
0.3	0.308	3.25	8 – 14.5	13 – 16.25
0.35	0.348	5.75	8 – 13.75	16 – 21.75
0.4	0.4	2.5	10 – 20	27 – 34.5
0.45	0.444	2.25	10 – 19	
0.5	0.5	2	13 – 25	
0.55	0.545	5.5	13 – 24	

Table 3
Frequencies and relative amplitudes used for waves in a nominal following current of 0.8 m/s. Each test is repeated five times.

Frequency	Relative input wave height							
[Hz]	0.25	0.5	1 (0.1 m)	1.5	1.75	2	2.25	4
0.308	X	X	X	X				
0.348			X					
0.4			X	X	X	X	X	
0.444			X					
0.5			X					
0.545			X					

2.5.2. Correcting sea states in the presence of current

For this study, regular waves are desired to be generated in 0.81 m/s of opposing and following relative current in the FloWave basin. This large current will significantly alter the form of the waves including wave height, length and associated velocities (see Jonsson et al., 1970). As the specifics of the wave phase is not important for these tests, and is hard to guarantee due to the presence of turbulence, only the regular wave amplitude needs to be corrected. This has been carried out iteratively in the frequency domain using Eq. (7), and applied to the identified wave snippets uninfluenced by reflections. Only the fundamental wave frequency, f_i, is considered in this correction process.

$$A(f_i)_{in,j+1} = [\frac{A(f_i)_{desired}}{A(f_i)_{measured,j}}]A(f_i)_{in,j} \tag{7}$$

where $A(f_i)_{in,j+1}$ is the input wave amplitude for frequency i and iteration $j+1$, $A(f_i)_{desired}$ is the desired value and $A(f_i)_{measured,j}$ is the measured value at iteration j.

2.6. Test plan

In this study monochromatic waves were used, as opposed to irregular waves, to enable a fundamental exploration of turbine response to a less complex wave–current velocity field. When using regular waves, it is therefore desirable to isolate the response to a variety of key wave parameters. The presented test plan primarily explores, separately, the influence of wave frequency, and amplitude, on the turbine response in both following and opposing waves.

Six target regular wave frequencies were chosen for exploration ranging from 0.31 Hz to 0.55 Hz tank scale. This corresponds, using Froude number similitude, to between 7.1 s and 12.5 s full-scale wave periods and hence are representative of commonly occurring surface gravity waves. As discussed in Section 2.5, the use of short wave segments means that it is desirable to have short repeat times, which in turn influences the available frequencies. The wave frequencies chosen for use are shown in Table 2 in combination with the sea state repeat time. Due to the short times achieved, for every test it was possible to identify a segment of good data containing an integer number of wave cycles. These snippet times are also displayed in Table 2 and as discussed, this improves the quality of the analysis significantly.

The frequency–amplitude combinations used for both following and opposing waves are presented in Tables 3 and 4, noting that five repeats are used for each combination. The different ranges of wave conditions used for opposing and following waves are due a combination of wavemaker limits and wave–current interaction effects. The target wave height for the constant amplitude–variable frequency tests is 0.1 m. Sea states underwent a correction procedure to obtain this amplitude using the methodology detailed in Section 2.5.2, and subsequently scaled using a linear gain factor to assess the influence of wave amplitude.

3. Theory and modelling

This section describes the calculation of turbine-related parameters, including basic parameters (Section 3.1), spectral identification of wave-induced power and thrust (Section 3.2), and the semi-empirical model used for prediction and comparison (Section 3.3).

Table 4
Frequencies and relative amplitudes used for waves in a nominal opposing current of 0.8 m/s. Each test is repeated five times.

Frequency	Relative input wave height							
[Hz]	0.25	0.5	1 (0.1 m)	1.5	1.75	2	2.25	4
0.308		X	X	X		X		X
0.348			X					
0.4		X	X	X		X		X

3.1. Basic turbine parameters

A number of variables are obtained directly from the data acquisition systems, see Section 2.3. This section covers those which are derived quantities.

To calculate instantaneous measured turbine power 'output', P, the torque, Q, can be used in combination with encoder measurements of angular position, θ, of the rotor:

$$P = Q\omega \quad ; \quad \omega = \frac{d\theta}{dt} \tag{8}$$

The theoretical power, P_{th}, can be described by:

$$P_{th} = \frac{1}{2} C_P \rho A U^3 \tag{9}$$

where ρ is the fluid density, $A = \pi R^2$ is the rotor plane area (with R as the rotor radius), U is the rotor-averaged current velocity (equivalent to Eq. (15) in waves), and C_P is the coefficient of power. C_P can be obtained experimentally by:

$$C_P = \frac{2P}{\rho A U^3} = \frac{2Q\omega}{\rho A U^3} \tag{10}$$

Similarly the coefficient of thrust, C_T, can be calculated as:

$$C_T = \frac{2\boldsymbol{T}}{\rho A U^2} \tag{11}$$

where $\boldsymbol{T}$ is the measured thrust. The values of C_P and C_T are characteristic of rotor performance. It is often of interest to calculate these quantities for a range of turbine speeds relative to the inflow velocity. This is often assessed using a tip-speed ratio, λ, defined in Eq. (12).

$$\lambda = \frac{\omega R}{U} \tag{12}$$

These calculated parameters are referred to throughout the article.

3.2. Spectral identification of wave-induced variations

As discussed in Section 2.5 it is desired to be able to identify the influence of waves on the turbine response in the frequency domain, rather than implementing time-domain approaches. This enables the influence of waves to be isolated from turbulence and bulk flow variations more effectively in the analysis. This section explores how this may be assessed for turbine power and thrust, and used to inform the subsequent analysis of experimental data.

Turbulence will be relatively insignificant when considering turbine response in the frequency bins corresponding to frequencies and harmonics of the regular waves. Indeed, Martinez et al. (2018) have shown that for the same turbine model and similar flow conditions, the thrust load associated with the fundamental frequency of the waves is about two order of magnitude higher than turbulence induced thrust. The effect of turbulence is therefore neglected for the purpose of the analysis. Under this approach, turbine power and thrust in waves can be described by Eqs. (13) and (14).

$$P_{U,w}(t) = \frac{1}{2} C_P \rho A [U^*(t)]^3 \tag{13}$$

$$\boldsymbol{T}_{U,w}(t) = \frac{1}{2} C_T \rho A [U^*(t)]^2 \tag{14}$$

where C_P and C_T are a function of $\lambda(U^*(t))$. $U^*(t)$ is the weighted rotor-averaged instantaneous current velocity including waves:

$$[U^*(t)]^n = \frac{1}{\int_{z_1}^{z_2} w(z)dz} \int_{z_1}^{z_2} [\bar{U(z)} + u_w(z,t)]^n w(z) dz \tag{15}$$

Table 5
Fourier coefficients for power and thrust. Shown up to sixth order with respect to φ.

Order	Power	Thrust
0	$\bar{U}^3 + \frac{3\bar{U}\boldsymbol{U}_{w,1}^2}{2} + \frac{3\boldsymbol{U}_{w,1}^2\boldsymbol{U}_{w,2}}{4} + \frac{3\bar{U}\boldsymbol{U}_{w,2}^2}{2}$	$\bar{U}^2 + \frac{\boldsymbol{U}_{w,1}^2}{2} + \frac{\boldsymbol{U}_{w,2}^2}{2}$
1	$\frac{3\boldsymbol{U}_{w,1}^2}{4} + 3\bar{U}^2\boldsymbol{U}_{w,1} + \frac{3\boldsymbol{U}_{w,1}\boldsymbol{U}_{w,2}^2}{2} + 3\bar{U}\boldsymbol{U}_{w,1}\boldsymbol{U}_{w,2}$	$2\bar{U}\boldsymbol{U}_{w,1} + \boldsymbol{U}_{w,1}\boldsymbol{U}_{w,2}$
2	$\frac{3\boldsymbol{U}_{w,2}^3}{4} + 3\bar{U}^2\boldsymbol{U}_{w,2} + \frac{3\bar{U}\boldsymbol{U}_{w,1}^2}{2} + \frac{3\boldsymbol{U}_{w,1}^2\boldsymbol{U}_{w,2}}{2}$	$2\bar{U}\boldsymbol{U}_{w,2} + \frac{\boldsymbol{U}_{w,1}^2}{2}$
3	$\frac{\boldsymbol{U}_{w,1}^3}{4} + \frac{3\boldsymbol{U}_{w,1}\boldsymbol{U}_{w,2}^2}{2} + 3\bar{U}\boldsymbol{U}_{w,1}\boldsymbol{U}_{w,2}$	$\boldsymbol{U}_{w,1}\boldsymbol{U}_{w,2}$
4	$\frac{3\boldsymbol{U}_{w,1}^2\boldsymbol{U}_{w,2}}{4} + \frac{3\bar{U}\boldsymbol{U}_{w,2}^2}{2}$	$\frac{\boldsymbol{U}_{w,2}^2}{2}$
5	$\frac{3\boldsymbol{U}_{w,1}\boldsymbol{U}_{w,2}^2}{2}$	
6	$\frac{\boldsymbol{U}_{w,2}^3}{4}$	

where $n = 3$ for power and $n = 2$ for thrust, and w is a weighting function, equal to the width of the rotor plane as a function of z position:

$$w(z) = 2\sqrt{R^2 - (z - z_o)^2} \tag{16}$$

where z_o is the z-position of the centre of the rotor, and $|z - z_o| < R$. u_w is wave-induced streamwise velocity, and $\bar{U}$ is the bulk flow velocity at a given z. For a regular wave of amplitude a and wavenumber K, the wave-induced velocity can be described at a given $x - z$ location, to second-order (Baddour and Song, 1990) as:

$$u_w(x, z, t) = \frac{gaK}{\sigma_r}\frac{\cosh(K(z+h))}{\cosh(Kh)}\sin(Kx - \sigma t) + \frac{3a^2K\sigma_r}{4\sinh^4(Kh)}\cosh(2K(z+h))\sin(2(Kx - \sigma t)) \tag{17}$$

where g is acceleration due to gravity, σ is the angular frequency and σ_r is the relative angular frequency i.e. the frequency observed in a reference frame moving at the same velocity as the mean current, x is the streamwise position, z is the vertical position in water depth h. Wavenumber and relative angular frequency are defined below:

$$\frac{\sigma}{K} = U + \sqrt{\frac{g}{K}\tanh(Kh)} \quad ; \quad \sigma_r = \sqrt{Kg\tanh(Kh)} \tag{18}$$

Defining $\boldsymbol{U}_{w,1} = \frac{gaK}{\sigma_r}\frac{\cosh(K(z+h))}{\cosh(Kh)}$, $\boldsymbol{U}_{w,2} = \frac{3a^2K\sigma_r}{4\sinh^4(Kh)}\cosh(2K(z+h))$ and $\varphi = Kx - \sigma t$, Eqs. (13) and (14) can be re-written as Eqs. (19) and (20) respectively.

$$P_{U,w}(t) = \frac{C_P\rho A}{2\int_{z_1}^{z_2} w(z)dz}\int_{z_1}^{z_2}[\bar{U(z)} + \boldsymbol{U}_{w,1}(z)\cos(\varphi) + \boldsymbol{U}_{w,2}(z)\cos(2\varphi)]^3 w(z)dz \tag{19}$$

$$\boldsymbol{T}_{U,w}(t) = \frac{C_T\rho A}{2\int_{z_1}^{z_2} w(z)dz}\int_{z_1}^{z_2}[\bar{U(z)} + \boldsymbol{U}_{w,1}(z)\cos(\varphi) + \boldsymbol{U}_{w,2}(z)\cos(2\varphi)]^2 w(z)dz \tag{20}$$

It is to be noted that alternative formulations exist for the computation of peak wave–current loads, such as that presented (Fernandez-Rodriguez et al., 2014). In this paper the viscous forces from waves and currents are decoupled, with the formulation adapted from an actuator disc model for the calculation of loads on jacket structures (Taylor et al., 2013).

To aid visualisation, it is useful to assume that fluctuations in $C_P(\lambda(t))$ and $C_T(\lambda(t))$ are negligible compared to wave-induced velocity contribution to power and thrust variation, i.e. can be approximated by $C_P(\bar{\lambda})$ and $C_T(\bar{\lambda})$. The frequency domain response can then be visualised using the Fourier series corresponding to the cube/square of the instantaneous total current velocity. As shown by the small variations in C_P and C_T around $\lambda = 7$ in Section 4.1, this assumption is valid when wave induced velocities are relatively small. From expansion of the velocity terms in Eqs. (19) and (20), the resulting Fourier series for wave-induced thrust and power spectra is presented in Table 5.

In addition to the symbolic representation of the wave-induced power and thrust harmonic content (Table 5), a visual representation is provided in Figs. 7 and 8. The relative value of the harmonics are shown compared to the mean value without waves. In these figures these harmonics are shown as a function of $\boldsymbol{U}_{w,1}/\bar{U}$ and $\boldsymbol{U}_{w,2}/\boldsymbol{U}_{w,1}$. This represents the relative magnitude of linear wave-induced velocity fluctuations to the mean velocity, and the relative value of the second-order wave terms relative to the fundamental. This essentially describes the harmonic response as a function of how large the waves are to the current, and how non-linear the waves are.

Using the visualisation presented in Figs. 7 and 8 a number of observations can be made. Assessing $n = 0$, it is clear that there is an increase in both mean power and thrust in the presence of waves. The wave contribution to mean power is quite large when wave-induced velocities are a significant proportion of the bulk flow, highlighting a potential benefit of waves at

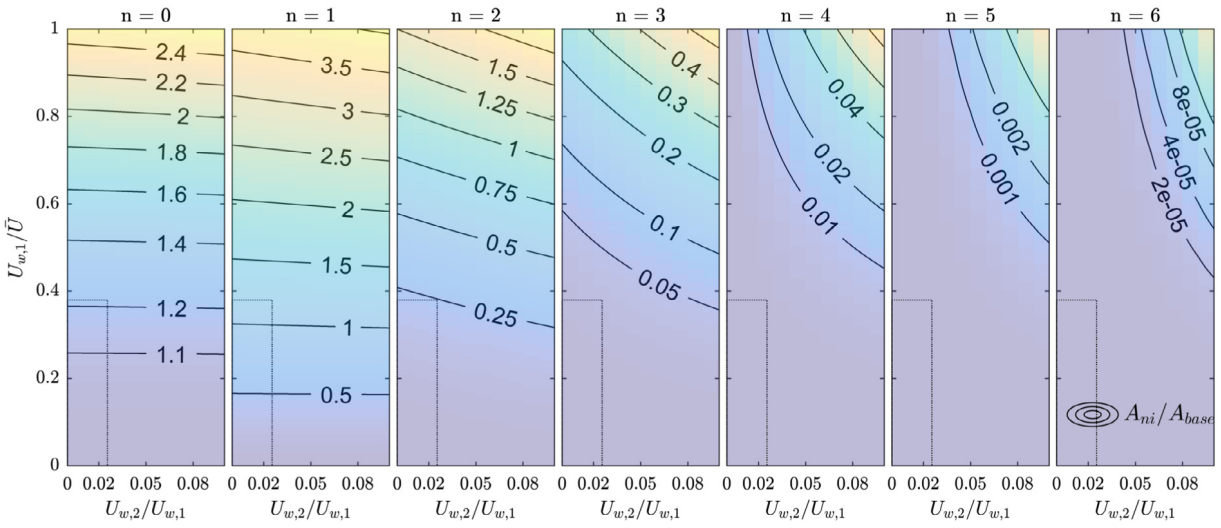

Fig. 7. Contours of theoretical Fourier coefficients in the power spectrum relative to the mean power without waves. Shown for various wave velocities relative to the mean flow, and various degrees of wave non-linearity. The region enclosed by dotted lines indicates that explored in the presented experimental test programme.

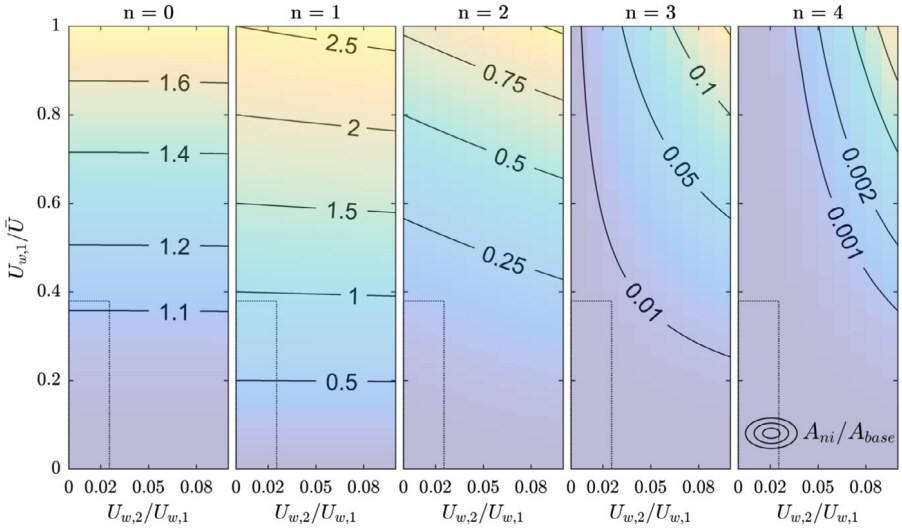

Fig. 8. Contours of theoretical Fourier coefficients in the thrust spectrum relative to the mean thrust without waves. Shown for various wave velocities relative to the mean flow, and various degrees of wave non-linearity. The region enclosed by dotted lines indicates that explored in the presented experimental test programme.

tidal sites despite the increased loading. Harmonic contribution to power and thrust variations decrease with n. For realistic cases, harmonics above 3rd order in power and 2nd order in thrust are negligible. It is also evident that these terms are not present when waves can be assumed linear i.e. when $\boldsymbol{U}_{w,2} = 0$ ($x = 0$ on Figs. 7 and 8). The inclusion of second-order waves, however, serves to increase the contribution from all harmonics, and as such load fluctuations will be under-estimated if these second-order effects are ignored.

3.2.1. Calculating maximum wave-induced power and thrust

Figs. 7 and 8 detail the expected relative magnitude of spectral peaks corresponding to harmonics of the wave frequency. This informs which components are of interest in understanding turbine response and need to be considered in the analysis. These harmonics can be used to identify the maximum wave-induced power and thrust values. To do this, the components of interest have been extracted from the measured force spectra (for thrust measurements up to fourth-order terms are included, whilst power includes up to sixth-order and wave-induced velocity up to second), before taking the maximum

value of an Inverse Fast Fourier Transform (IFFT) including only these components. This approach effectively isolates wave-induced maxima from those incorporating turbulence. As these maximum values are crucial for design, the results presented in Sections 4.2 and 4.3 include the response to the fundamental wave frequency, along with these maximum wave-induced values.

3.3. Semi-empirical model

The theory presented in Section 3.2 is used to understand the harmonic response of the turbine to second order waves, which aids in the approach to analyse the experimental results; the main focus of the article. However, in addition, it can also be adapted to estimate power and thrust providing a number of simplifying assumptions (in addition to pseudo-stationarity) can be made. Namely that:

1. Reference velocity as measured in the absence of the turbine is a good approximation for wave–current interaction calculations
2. Effects of dynamic stall can be neglected
3. Turbulence can be ignored
4. Effects of vertical component of wave-induced velocity can be neglected

For the generation of Figs. 7 and 8, it was not necessary to know the absolute values of parameters as relative values of power and thrust are presented for visualisation. To obtain absolute estimated values of power and thrust to compare with measurements, however, estimates of $\bar{U}$, $C_P(t)$, $C_T(t)$, and $U^*(t)$ are required.

For estimating $C_P(t)$ and $C_T(t)$, pseudo-stationarity is assumed. Interpolated values are obtained from current only tests, for every time step, as a function of the instantaneous tip speed ratio. To obtain this tip speed ratio, and to estimate wave-induced loads on the turbine (K dependency on U) it is required to have good estimates for $U(z)$. An undisturbed reference velocity ($\bar{U}(z)$) has been used for all calculations, ensuring that C_P and C_T, along with the velocity used for power and thrust calculations are consistent. This is analogous to predicting full scale turbine loads based on pre-deployment site characterisation measurements.

Additionally, from Noble et al. (2015) it is also known that the velocity without a turbine present obeys a 1/15th power law. This has been incorporated into the reference $U(z)$ estimates, using measurements at tip height (z_{base}) as the base velocity and Eq. (21):

$$\bar{U}(z) = \bar{U}(z_{base})\left(\frac{z_{base} - z}{z_{base}}\right)^{1/15} \tag{21}$$

This semi-empirical model is presented in conjunction with the experimental results to provide comparison. The procedure used to estimate wave-induced power and thrust is as follows:

1. Obtain value of a from FFT of wave gauge data located above turbine: snippet used including only high quality data, which is a multiple of the repeat time
2. Use a to predict $U_{w,1}(z)$ and $U_{w,2}(z)$
   (a) K calculated using the $\bar{U}$ at tip height, with Eq. (18)
   (b) Eq. (17) used to calculate $U_{w,1}(z)$ and $U_{w,2}(z)$ at various z positions spanning the rotor plane
3. Eq. (21) used to obtain $U(z)$
4. Weighted rotor-average values of total velocity ($\sqrt{U^2}$ and $\sqrt[3]{U^3}$) computed from Eq. (15) for every time-step and calculate instantaneous λ values
5. Estimates of $C_P(t)$ and $C_T(t)$ are obtained by interpolating the measured steady state data, using λ from each time step (with ω = 90rpm for the presented tests)
6. Wave-induced power and thrust variations computed using Eqs. (19) and (20)
7. Spectral analysis applied to the resulting time-series allows direct comparisons to frequency domain power and thrust variations obtained from experiments

4. Results

Prior to presenting the results from the main experimental programme, baseline turbine data is shown in Section 4.1. The results of the frequency-domain turbine response analysis are then presented. Wave-induced fluctuations in streamwise velocity, turbine power and thrust are presented as a function of wave amplitude and frequency in Sections 4.2 and 4.3 respectively.

In Sections 4.2 and 4.3, fluctuations at the fundamental wave frequency along with wave-induced maxima are shown. The wave-induced change to the mean values of power and thrust are not presented as it is not possible to isolate wave-induced changes to the mean values from changes due to current velocity variations. The short analysis times used for the 'snippet' approach result in a variable value of the mean current velocity. As the $n = 0$ contribution is very sensitive to this (see Table 5), the mean values of power and thrust also vary significantly due to current alone. The time period required to have a stable mean velocity at FloWave is around a minute (see Sutherland et al., 2017) and hence a significantly longer time period that is currently possible would be required to obtain a reasonable comparison.

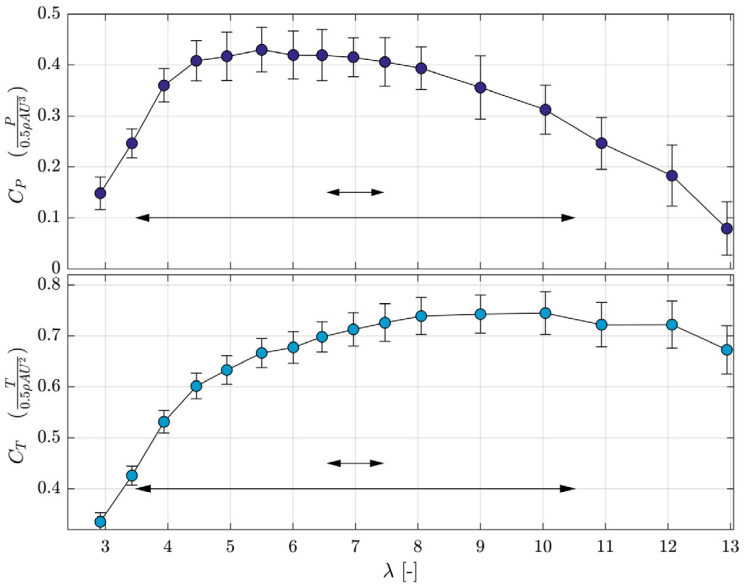

Fig. 9. Power and thrust coefficients as a function of tip speed ratio, with $U_{ref} = 0.81$ m/s. Error bars denote the standard deviation observed in each 5 min test. The two sets of arrows indicate the minimum and maximum range of expected instantaneous tip speed ratios as a result of waves for the tests presented.

4.1. Baseline turbine information: Power and thrust

The baseline rotor behaviour in current-only conditions is well described by the power and thrust coefficients, C_P and C_T (Eqs. (10) and (11)). These are shown for a wide range of λ values in Fig. 9. All data were obtained in a reference current velocity of 0.81 m/s, and different λ values were obtained by varying the rotational speed of the turbine. The value of the current velocity used to calculate the C_P and C_T values from Eqs. (10) and (11) was taken as the expected mean weighted velocity over the rotor plane. This has been informed from long-run (900 s) ADV measurements at hub height without the turbine present along with an assumed 1/15th (Noble et al., 2015) power law: resulting in a value of 0.81 m/s. It is worth noting that throughout the tests presented the mean (over each test) correlation values and signal-to-noise ratios of the ADV were kept above 95% and 20 respectively.

The expected instantaneous λ range for the smallest and largest waves are indicated by the arrows on Fig. 9. The small arrow indicates the expected range of λ values in the smallest wave tested, with the large arrow indicating the range associated with the largest wave. It is evident that for those conditions which induce small variations in λ, the variations in effective C_P and C_T are relatively small and as such are negligible compared with the wave-induced velocity contribution to power and thrust variation. However, for the larger waves this is no longer a valid assumption, and hence the interpolation method described in Section 3.3 is required to obtain estimated values.

The experimentally obtained mean values of power and thrust (at scale) at $\lambda = 7$ are 119 W and 258 N respectively, and put the wave-induced variations presented in Sections 4.2 and 4.3 into perspective.

4.2. Effect of wave amplitude

To demonstrate how surface elevations and corresponding turbine response are identified in the frequency domain, an example is given in Fig. 10. This shows the time and frequency domain equivalents of the surface elevation and resulting turbine power output for an amplitude sweep in 0.4 Hz opposing waves. From Fig. 10, it is evident that the magnitude of the surface elevations and wave-induced power fluctuations are well represented in the frequency domain. Power is negatively correlated with surface elevation due to the direction of propagation of the waves (opposing). Second-order contribution to waves is also evident from the peak at 0.8 Hz in the surface elevation spectra, which will impact the magnitude of the expected peak loads and power fluctuations of the turbine. Additional 'ripples' are noted in the time-series of power, which correspond to blade tower shadow effects occurring three times per revolution.

As described in Tables 3 and 4, a range of wave amplitudes were generated for 0.31 Hz and 0.4 Hz waves, in both opposing and following conditions. The magnitude of the wave-induced variations are shown in Figs. 11 and 12 for 0.31 Hz and 0.4 Hz respectively. These show wave-induced variations in thrust, power, and streamwise velocity, U, 2D upstream of the turbine (as depicted in Fig. 4). The magnitude of turbine response at the fundamental wave frequency and maximum wave induced values are presented (see Section 3.2.1), with the difference between the two indicating the extent of higher order response

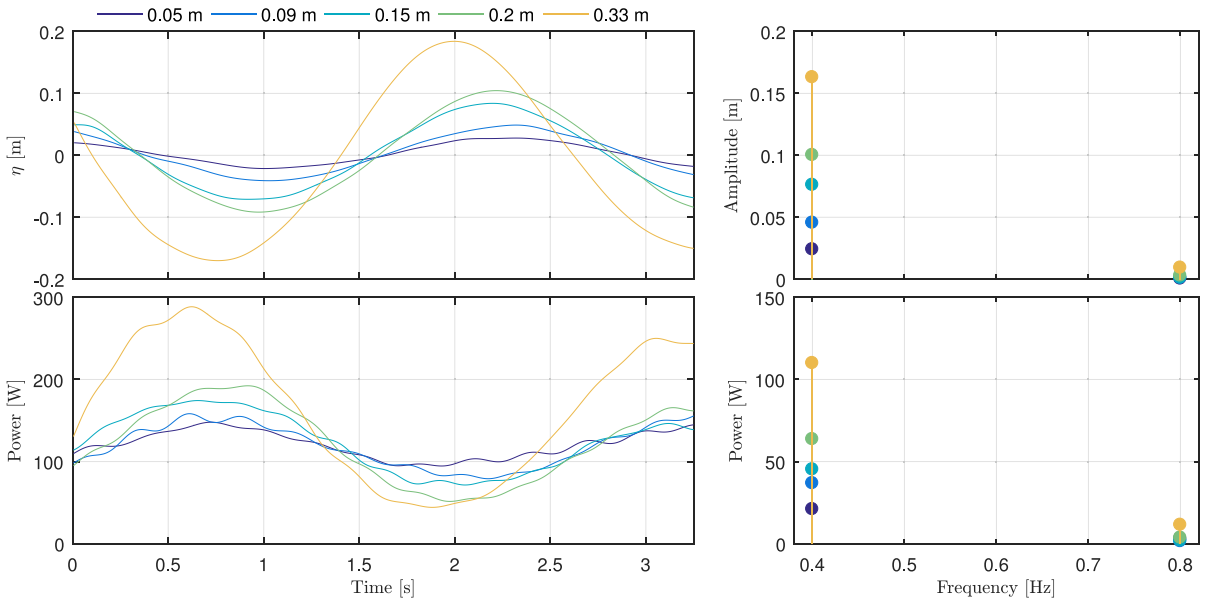

Fig. 10. Frequency and time-domain examples of surface elevation and corresponding variations in power. One repeat of each of the 5 amplitudes at 0.4 Hz shown in opposing current. Time-series data is low pass filtered at 4 Hz to aid visibility.

for the different wave frequencies. Also shown on the right hand axis of Figs. 11 and 12 is the percentage variations relative to current only mean values.

As expected, lower frequency–higher amplitude waves cause larger fluctuations. Some of these large wave conditions induce very significant variations in velocity and subsequently in turbine loads and power, with the largest 0.31 Hz opposing wave inducing power and thrust variations exceeding current only values by 160% and 65% respectively. For a given wave amplitude and frequency, it is observed that waves in following current conditions induce larger variations in power and thrust. This is expected due to the smaller associated K values, and corresponding reduced depth attenuation of wave-induced velocity components. Also as predicted, from Fig. 7, greater higher-order content is observed in the power than is seen in thrust, indicated by the difference between fundamental and maximum response. For all but the largest–lowest frequency waves, however, the response at the fundamental frequency largely describes the turbine behaviour in waves. This is due to the small relative magnitude of $U_{w,1}$ to $\bar{U}$, meaning that perturbations around the mean velocity are reasonably approximated as linear (see Figs. 7 and 8).

Also shown in Figs. 11 and 12 is the repeatability for the experimentally derived response at the fundamental. Error bars denote the standard deviation between the five repeats (shown for fundamental response only for clarity). It is noted that the extracted wave-induced turbine power and thrust are very repeatable, even though there is reduced repeatability in the wave-induced velocities.

Despite the semi-empirical model omitting various physical features of the turbine behaviour, it is evident that the pseudo-stationary approach predicts both the first-order wave-induced fluctuations and the peak wave-induced power and thrust reasonably well. This suggests it may be a useful practical approach in predicting turbine loads. However, it is to be noted that its validity may be limited to the high λ values used in the experiments, which is discussed further in Section 5.2.

4.3. Effect of wave frequency

An example of the time and frequency domain response to differing wave frequencies are shown in Fig. 13 for the frequency sweep in following current. It is clear that the magnitude of the oscillations observed in the time domain are captured spectrally. Comparing between the surface elevation and the power, it is evident that lower frequency result in increased loading due to the lower K values, and reduced attenuation with depth. It is worth noting that in this example, waves are following the current, and as such power is now positively correlated to the surface elevation, unlike the opposing current example shown in Fig. 10.

The turbine response to different wave frequencies in both opposing and following current conditions is shown in Fig. 14. In addition to wave-induced variations in thrust, power, and streamwise velocity, U, wave amplitudes as measured above the turbine are shown. It is evident, from Fig. 14 that the effect of frequency, within this range, is quite limited. Indeed, comparing frequency response in complete isolation is somewhat challenging as the amplitudes of the waves were not precisely equal. However, despite having smaller wave amplitudes, a larger response to 0.31 Hz and 0.35 Hz following waves is observed for turbine power, thrust and U. This is due to decreased velocity attenuation with depth for lower frequencies (lower K

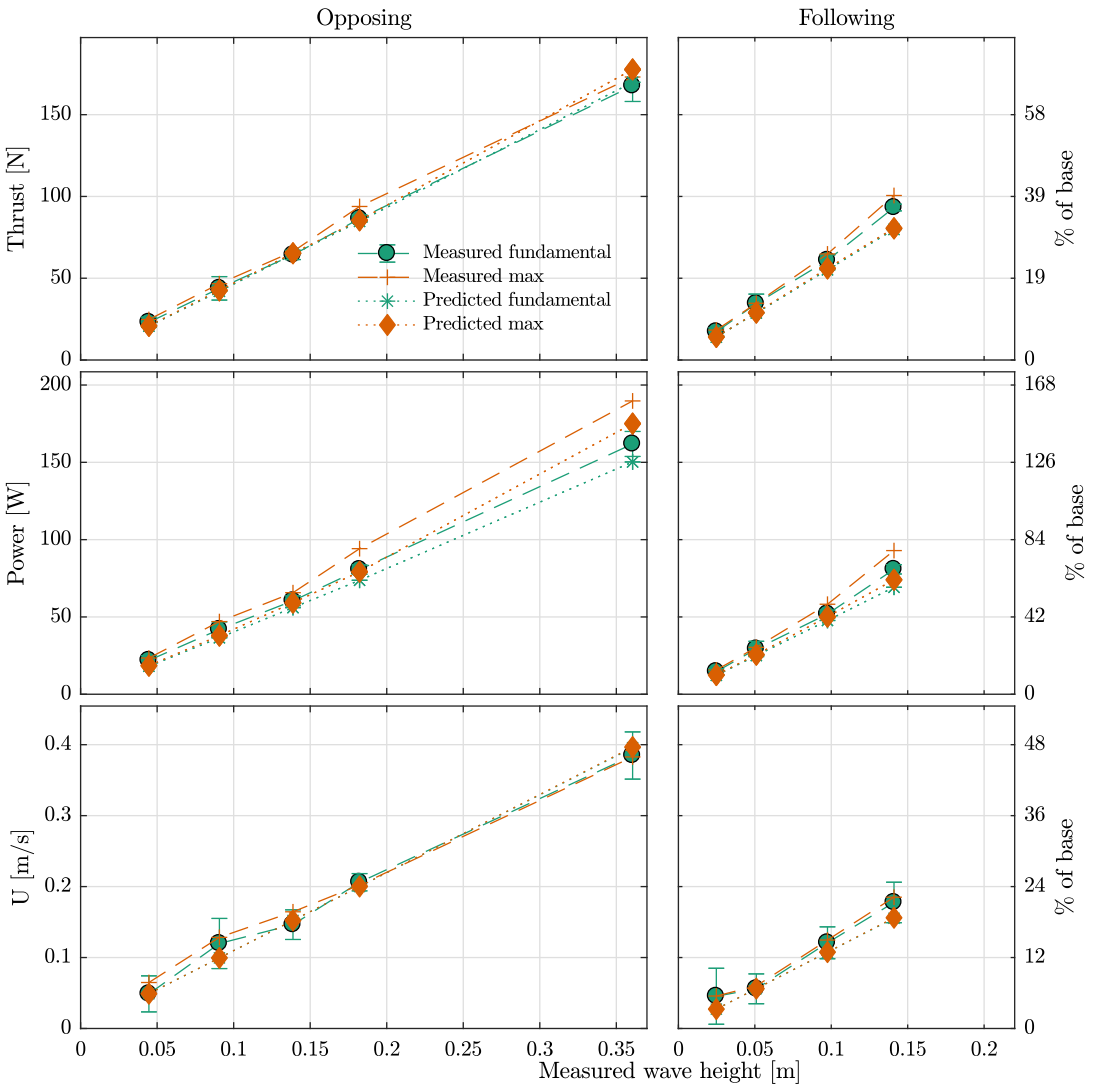

Fig. 11. Wave induced fluctuations in various parameters as a function of wave amplitude. Shown for opposing and following waves at 0.31 Hz in a mean current velocity of 0.81 m/s, along with predicted values. Error bars denote the standard deviation between the 5 repeats. Left hand axis shows absolute wave-induced fluctuations, whilst right hand axis shows these variations as a percentage of current only values.

values), thus inducing larger total velocity fluctuations when averaged over the rotor plane. This is also the explanation for the significantly reduced turbine response in opposing wave conditions. The opposing current increases K and hence causes greater attenuation with depth.

Similar to the results for wave amplitude, the semi-empirical model provides reasonable estimates of the fundamental and peak wave-induced variations in power and thrust to a variety of wave frequencies of (near) constant amplitude. The discrepancies that do exist may be a result of a number of assumptions/simplifications. This, along with other potential reasons are discussed further in Section 5.2.

5. Discussion

5.1. Assessment of frequency-domain analysis approach

To effectively isolate the frequency domain response of the turbine in regular waves a combined wave generation–analysis strategy was implemented: wave frequencies were chosen specifically to facilitate spectral analysis. This ensured that a whole number of incident waves were analysed for each frequency–height–direction combination, with 5 repeats used to verify the consistency of the procedure. The repeatability was found to be extremely high, indicated by the low standard deviations in fundamental response shown in Figs. 11, 12 and 14. This demonstrates that the approach was effective in

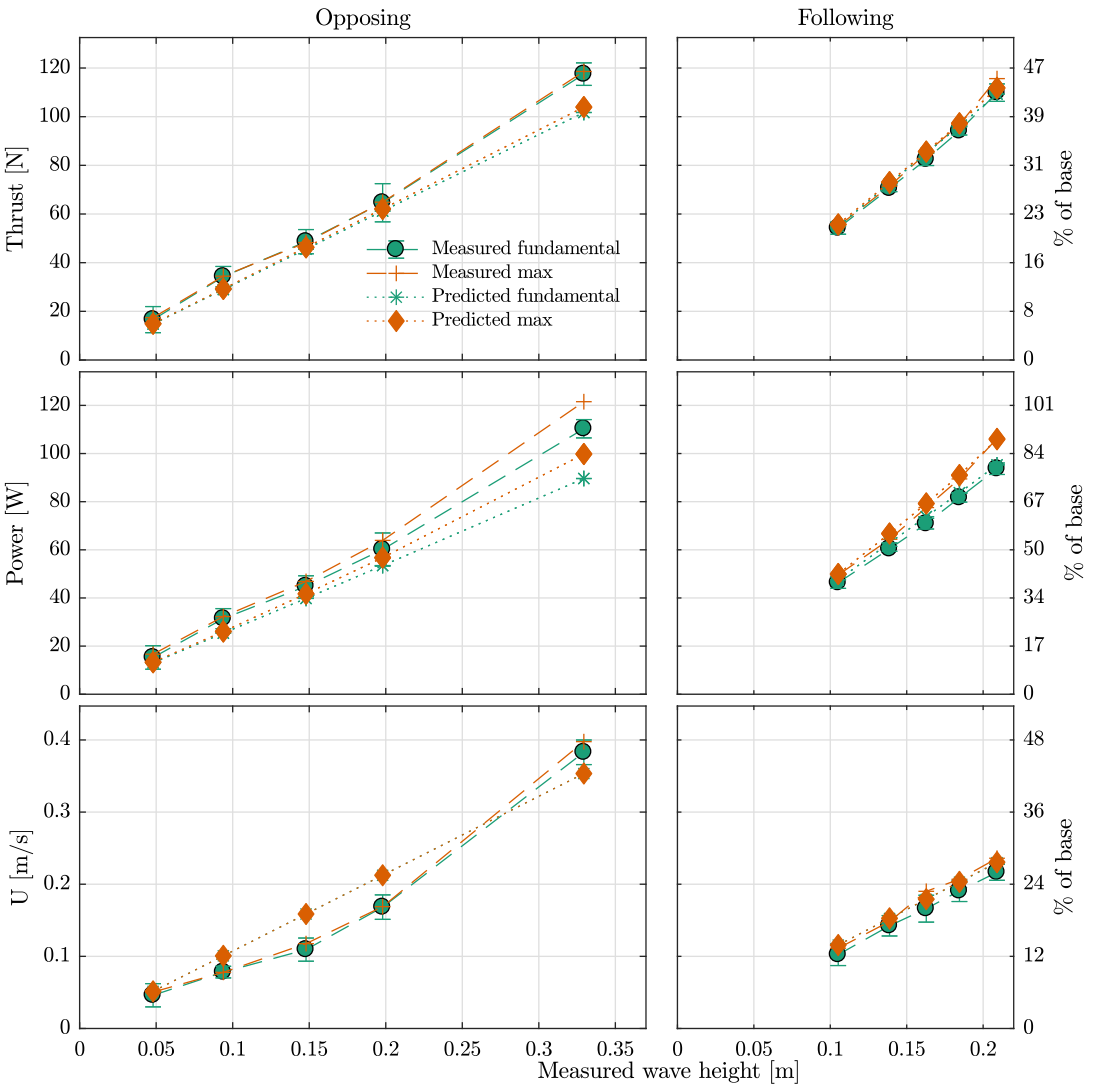

Fig. 12. Wave induced fluctuations in various parameters as a function of wave amplitude. Shown for opposing and following waves at 0.4 Hz in a mean current velocity of 0.81 m/s, along with predicted values. Error bars denote the standard deviation between the 5 repeats. Left hand axis shows absolute wave-induced fluctuations, whilst right hand axis shows these variations as a percentage of current only values.

isolating wave-induced turbine response from the influence of turbulence and wave reflections, and that perhaps for future tests the number of repeats can be reduced. This suggests that this methodology can be implemented to rapidly assess wave-induced loads on bottom-mounted tidal turbines, requiring very short time-frames to assess combinations of wave frequency, amplitude, and relative wave–current angle. The analysis approach presented, considering all relevant harmonics of the wave frequency, is also crucial to the method's success and ensures that peak wave-induced loads are not under-estimated.

It is evident from Figs. 11, 12 and 14 that, in general, the experimentally obtained wave-induced power and thrust variations were larger than predicted from the model. Although there are a number of reasons why the discrepancy may result from the model, as discussed further in Section 5.2, it also may suggest that the contribution of turbulence to the frequency bins corresponding to the waves may be non-negligible resulting in experimentally obtained wave-induced variations being over-represented. It is estimated, from baseline turbulence measurements, that the turbulent amplitude associated with the frequency bins of velocity corresponding to the wave fundamental frequency is between 0.01 m/s and 0.03 m/s depending on the test length and frequency. As a result of the differing phases of the stochastic turbulence and deterministic wave, these will combine differently depending on the precise nature of the turbulence measured in each repeat snippet. It can therefore be inferred that the effect of this turbulence on the response at the fundamental wave frequency is fairly negligible as the repeatability is high. In general this effect will be negligible when the wave amplitudes are large, however may cause significant discrepancy for tests with small waves, and for the extraction of higher wave

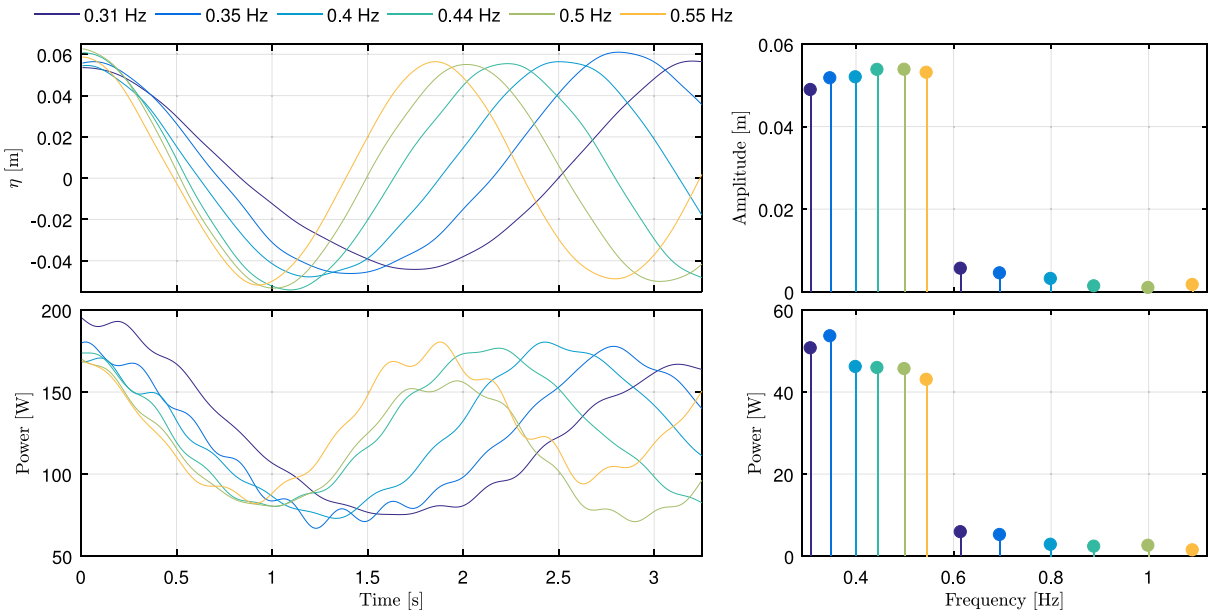

Fig. 13. Frequency and time-domain examples of surface elevation and corresponding variations in power. Shown for 6 frequencies with a single target amplitude, in following current. Time-series data is low pass filtered at 4 Hz to aid visibility.

harmonics. The apparent wave-induced loads and power will be artificially increased relative to the theory as the wave gauge measurements will be unaffected.

5.2. Applicability of semi-empirical model

Reasonable agreement between the semi-empirical model and experimental results was found in Sections 4.2 and 4.3. Mean errors in estimated fundamental power and thrust response were found to be less than 5% and 3% respectively, with corresponding mean peak wave-induced response errors less than 7% and 5%. The largest individual errors are a little over 20%, however, in general this approach proved relatively effective, despite a number of simplifying assumptions (see Section 3.3). The fact that the model provides good predictions despite these assumptions suggests that this simple and fast approach may be a useful tool for TST developers to superimpose wave field scatter plots on tidal flow data to obtain load and power fluctuation estimates, and only requires a well understood map of C_P and C_T to provide reasonable results. It is expected, however, that some of the assumptions made in the model are valid for these experiments yet may not be for other combinations of wave–current conditions and turbine operating point. It is therefore important to understand the limit of their validity.

One of the most significant of these assumptions is that a single estimated velocity can be used for the wave–current-turbine interaction calculations. It appears not to be too significant for the conditions presented in this paper, however, adaptations would clearly be required for conditions where the turbine more significantly alters the flow. This would have the effect of reducing the effective velocity for the wave–current interaction calculations, thus altering the wave heights, wavenumbers and corresponding TST loads.

As the model presented uses a pseudo-stationary, rotor-averaged approach, dynamic effects are ignored including the effect of dynamic stall. This also could be one of the main reasons for the mismatch between the theory presented and the experimental results. However, the high λ values used in this work mean this is unlikely to be significant other than for the largest wave cases. For turbines operating at lower λ values, however, this effect may not be ignored, and the reader is pointed to Milne et al. (2015) for more details on this phenomenon.

5.2.1. Suitability of linear wave theory

For the wave–current conditions presented it has been noted that, in general, there are only very small differences between estimated turbine power and thrust when using linear or second order wave–current theory. This is not the case for the very large, low frequency waves where the second-order velocity components are still appreciable lower down in the water column. The largest discrepancy is therefore observed for the 0.31 Hz–0.37 m (height) wave. For this wave condition, there is approximately a 2% reduction in the estimate of peak power, and 1.4% reduction in peak thrust. Although these errors are not particularly large, they serve to further under-predict the peak wave-induced loads. It is therefore a prudent approach to include second-order wave-induced velocities for TST load calculations.

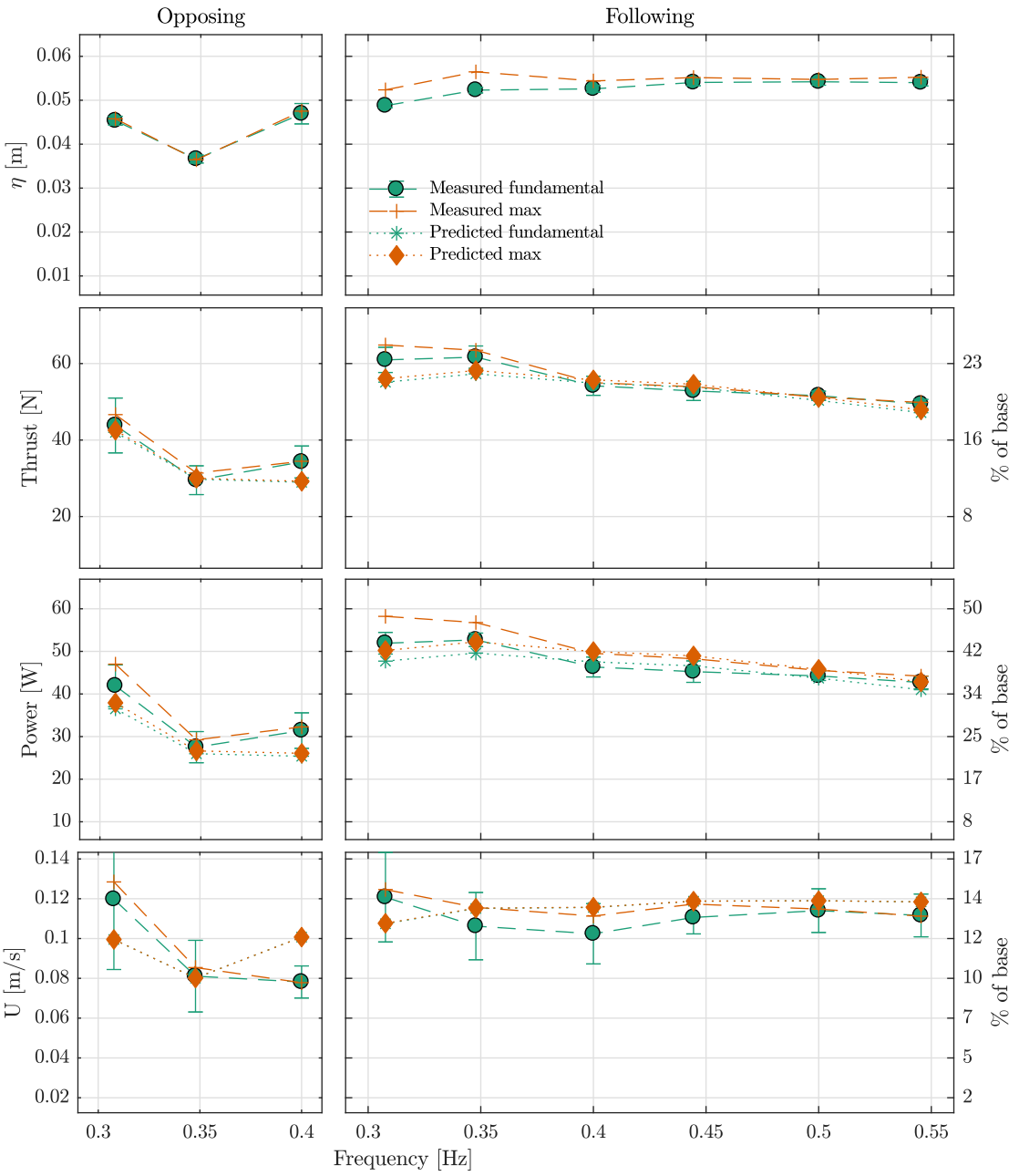

Fig. 14. Wave induced fluctuations in various parameters as a function of wave frequency. Shown for opposing and following waves in a mean current velocity of 0.81 m/s. Error bars denote the standard deviation between the 5 repeats. Left hand axis shows absolute wave-induced fluctuations, whilst right hand axis shows these variations as a percentage of current only values.

6. Conclusions

This paper presents an experimental investigation into the power and thrust response of a 1:15 scale tidal turbine under a wide range of regular wave conditions in a constant current velocity. The influence of wave amplitude and frequency on the power and thrust variations in both following and opposing conditions are assessed; utilising a frequency domain analysis approach to isolate the wave-induced components. Special care is taken to ensure high quality of the frequency analysis by avoiding frequency spilling and the effect of wave reflection. Large variations are observed which increase with wave amplitude, decrease with frequency, and are larger for following current conditions. For the range of conditions tested, peak values of thrust and power exceed current only values by between 7%–65% and 13%–160% respectively.

The frequency-domain analysis approach is shown to be effective, isolating wave-induced components from turbulence and bulk flow variations. From the theoretical analysis, considering second-order waves, it is noted that although high-order harmonic response is expected, the magnitude of these are negligible above third-order in power and second-order in thrust. There is good agreement between experimental results and the theory presented; providing reasonable estimates of both the fundamental and peak response of turbine power and thrust to waves. This work hence increases the understanding of fundamental wave–current-turbine interaction, demonstrates an effective methodology for isolating these effects experimentally, and details the applicability of a computationally efficient semi-empirical methods for analysis.

Acknowledgements

The authors are grateful for financial support from the UK Engineering and Physical Sciences Research Council through FloWTurb: Response of Tidal Energy Converters to Combined Tidal Flow, Waves and Turbulence (EP/N021487/1) and SuperGen UK Centre for Marine Energy Research, UK (EP/M014738/1). The authors also acknowledge support from the EPSRC, UK for funding the FloWave Ocean Energy Research facility (EP/I02932X/1). The authors are extremely grateful to the staff at the FloWave facility, in addition to the FloWTurb project team, for making this research possible.

References

Atlantis, 2017. MeyGen – Tidal Projects – Atlantis Resources. https://www.atlantisresourcesltd.com/projects/meygen/. URL https://www.atlantisresourcesltd.com/projects/meygen/.

Baddour, R.E., Song, S.W., 1990. Interaction of higher-order water waves with uniform currents. Ocean Eng. 17 (6), 551–568.

Barltrop, N., Varyani, K.S., Grant, A., Clelland, D., Pham, X., 2006. Wave–current interactions in marine current turbines. Proc. Inst. Mech. Eng. Part M J. Eng. Marit. Environ. 220 (4), 195–203, URL http://journals.sagepub.com/doi/101243/14750902JEME45.

De Jesus Henriques, .T.A., Tedds, S.C., Botsari, A., Najafian, G., Hedges, T.S., Sutcliffe, C.J., Owen, I., Poole, R.J., 2014. The effects of wave–current interaction on the performance of a model horizontal axis tidal turbine. Int. J. Marine Energy 8, 17–35, URL http://dx.doi.org/101016/j.ijome.201410002.

Draper, S., Adcock, T.A.A., Borthwick, A.G.L., Houlsby, G.T., 2014. Estimate of the tidal stream power resource of the Pentland Firth. Renew. Energy 63, 650–657, URL http://dx.doi.org/101016/j.renene.201310015.

Draycott, S., Steynor, J., Davey, T., Ingram, D.M., 2018. Isolating incident and reflected wave spectra in the presence of current. Coastal Eng. J. 1–12.

Draycott, S., Sutherland, D., Steynor, J., Sellar, B., 2017. Re-creating waves in large currents for tidal energy applications. Energies 10, 1838.

Faudot, C., Dahlhaug, O.G., jan, 2012. Prediction of wave loads on tidal turbine blades. Energy Procedia 20, 116–133, URL http://linkinghub.elsevier.com/retrieve/pii/S1876610212007448.

Fernandez-Rodriguez, E., Stallard, T.J., Stansby, P.K., 2014. Experimental study of extreme thrust on a tidal stream rotor due to turbulent flow and with opposing waves. J. Fluids Struct. 51, 354–361, URL http://dx.doi.org/101016/j.jfluidstructs.201409012.

Galloway, P.W., Myers, L.E., Bahaj, A.S., mar, 2014. Quantifying wave and yaw effects on a scale tidal stream turbine. Renew. Energy 63 (2014), 297–307, URL http://linkinghub.elsevier.com/retrieve/pii/S0960148113004977.

Gaurier, B., Davies, P., Deuff, A., Germain, G., 2013. Flume tank characterization of marine current turbine blade behaviour under current and wave loading. Renew. Energy 59, 1–12, URL http://dx.doi.org/101016/j.renene.201302026.

Guo, X., Yang, J., Gao, Z., Moan, T., Lu, H., 2018. The surface wave effects on the performance and the loading of a tidal turbine. Ocean Eng. 156 (May), 120–134, URL https://doi.org/101016/j.oceaneng.201802033.

IEC TS 62600-200:2013, 2013. Marine energy - Wave, tidal and other water current converters. Part 200: Electricity producing tidal energy converters - Power performance assessment. Standard, International Electrotechnical Commission, Geneva, Switzerland.

IEC TS 62600-201:2015, 2015. Marine energy - Wave, tidal and other water current converters. Part 201: Tidal energy resource assessment and characterization. Standard, International Electrotechnical Commission, Geneva, Switzerland.

Ingram, D., Wallace, R., Robinson, A., Bryden, I., 2014. The design and commissioning of the first, circular, combined current and wave test basin. In: Proceedigns of the OCEANS 2014, pp. 1–7.

Jonsson, I.G., Skougaard, C., Wang, J.D., 1970. Interaction between waves amd currents. Coastal Eng. Proc. 1 (12).

Lust, E.E., Luznik, L., Flack, K.A., Walker, J.M., Van Benthem, .M.C., 2013. The influence of surface gravity waves on marine current turbine performance. Int. J. Marine Energy 3-4, 27–40, URL http://dx.doi.org/101016/j.ijome.201311003.

Luznik, L., Flack, K.A., Lust, E.E., Taylor, K., 2013. The effect of surface waves on the performance characteristics of a model tidal turbine. Renew. Energy 58, 108–114, URL http://dx.doi.org/10.1016/j.renene.2013.02.022.

MacEnri, J., Reed, M., Thiringer, T., 2013. Influence of tidal parameters on SeaGen flicker performance. Phil. Trans. R. Soc. A 371 (1985).

Martinez, R., Payne, G.S., Bruce, T., 2018. The effects of oblique waves and currents on the loadings and performance of tidal turbines. Ocean Eng. 164, 55–64, URL http://www.sciencedirect.com/science/article/pii/S0029801818309296.

MayGen Ltd., 2016. MeyGen Tidal Energy Project Phase 1. Project Environmental Monitoring Programme, Technical Report. Tech. Rep. MEY-1A-70-HSE-018-I-PEMP.

Milne, I.A., Day, A.H., Sharma, R.N., Flay, R.G.J., 2013. Blade loads on tidal turbines in planar oscillatory flow. Ocean Eng. 60 (Supplement C), 163–174, URL http://www.sciencedirect.com/science/article/pii/S0029801812004465.

Milne, I.A., Day, A.H., Sharma, R.N., Flay, R.G., 2015. Blade loading on tidal turbines for uniform unsteady flow. Renew. Energy 77, 338–350.

Milne, I.A., Sharma, R.N., Flay, R.G.J., 2017. The structure of turbulence in a rapid tidal flow. Proc. R. Soc. A 473 (2204), URL http://rspa.royalsocietypublishing.org/content/473/2204/20170295.

Milne, I.A., Sharma, R.N., Flay, R.G.J., Bickerton, S., 2010. The Role of Waves on Tidal Turbine Unsteady Blade Loading. In: 3rd International Conference on Ocean Energy (1), pp. 1–6. URL https://www.google.co.uk/webhp?sourceid=chrome-instant&ion=1&espv=2&ie=UTF-8{#}q=effect+of+turbulence+in+unsteady+blade+loads&spell=1.

Noble, D.R., Davey, T., Smith, H.C.M., Kaklis, P., Robinson, A., Bruce, T., 2015. Characterisation of spatial variation in currents generated in the FloWave Ocean Energy Research Facility. In: Proceedings of the 11th European Wave and Tidal Energy Conference. Nantes, France, pp. 1–8.

Parkinson, S.G., Collier, W.J., 2016. Model validation of hydrodynamic loads and performance of a full-scale tidal turbine using Tidal Bladed. Int. J. Marine Energy 16, 279–297.

Payne, G.S., Stallard, T., Martinez, R., 2017. Design and manufacture of a bed supported tidal turbine model for blade and shaft load measurement in turbulent flow and waves. Renew. Energy 107, 312–326.

Payne, G., Taylor, J., Ingram, D., 2009. Best practice guidelines for tank testing of wave energy converters. J. Ocean Technol. 4 (4), 38–70.

Sutherland, D.R.J., Noble, D.R., Steynor, J., Davey, T.A.D., Bruce, T., 2017. Characterisation of current and turbulence in the flowave ocean energy research facility. Ocean Eng. 139, 103–115.

Tatum, S.C., Frost, C.H., Allmark, M., O'Doherty, D.M., Mason-Jones, A., Prickett, P.W., Grosvenor, R.I., Byrne, C.B., O'Doherty, T., 2016. Wave–current interaction effects on tidal stream turbine performance and loading characteristics. Int. J. Marine Energy 14, 161–179, URL http://dx.doi.org/10.1016/j.ijome.2015.09.002.

Taylor, P.H., Santo, H., Choo, Y.S., 2013. Current blockage: Reduced Morison forces on space frame structures with high hydrodynamic area, and in regular waves and current. Ocean Eng. 57, 11–24, URL http://dx.doi.org/10.1016/j.oceaneng.2012.08.006.

The Crown Estate, 2012. UK Wave and Tidal Key Resource Areas Project - Summary Report. Tech. rep..